DOI: 10.1021/cg900732h

CRYSTAL GROWTH & DESIGN Article
XXXX, Vol. XXX
000–000

Growth Model of MOCVD Polycrystalline ZnO

S. Nicolay,* S. Fay, and C. Ballif

Ecole Polytechnique Fédérale de Lausanne (EPFL), Institute of Microengineering (IMT), Photovoltaics and thin film electronics laboratory EPFL-STI-IMT-NE, PV-LAB, Rue Breguet 2, CH-2000 Neuchâtel, Switzerland

Received June 30, 2009; Revised Manuscript Received August 19, 2009

ABSTRACT: A growth model for the low pressure chemical vapor deposition (LPCVD) of polycrystalline ZnO thin films is proposed. This model is based on experimental observations of the surface morphology and crystallographic orientations of the layers at different thicknesses and growth temperatures. It is shown that the films preferred orientation evolves from *c*-axis to *a*-axis as the growth temperature is increased from 110 to 220 °C and then goes back to *c*-axis at 380 °C. At the same time, when the film thickness increases, the surface morphology evolves from small rounded grains to large pyramids at a growth temperature of 150 °C. The selection of various preferential orientations under different deposition conditions is attributed to growth competition between clusters initially formed with different crystallographic orientations.

Introduction

Because of its wide bandgap and high exciton binding energy, zinc oxide (ZnO) has attracted much attention in the past years, notably for opto-electronic applications such as UV diodes and lasing devices operating at room temperature.[1] Yet another important prospect for ZnO is its use as a transparent conductive oxide (TCO) for thin film (TF) solar cells applications.[2] Regarding the ZnO growth, it can be synthesized by various techniques such as metal organic chemical vapor deposition (MOCVD),[3] sputtering,[4] molecular beam epitaxy (MBE)[5] or even sol−gel methods.[6] For photovoltaic applications, one of the preferred deposition techniques is the low pressure chemical vapor deposition (LPCVD). When used as front TCO electrodes, such LPCVD grown layers lead to high currents and efficiencies for amorphous,[7] microcrystalline solar cells and a high matched current can be obtained in tandem micromorph cells.[8,9] Indeed, ZnO layers grown with this technique, under given growth conditions, are polycrystalline films constituted of large grains with a pronounced preferential orientation (PO) along the *a*-axis.[10] This leads to natural staircase-faced pyramids at the top of the film, which gives to LPCVD grown ZnO good light scattering ability, a prerequisite for TF solar cell applications. Indeed, because of the relatively small values of the amorphous and microcrystalline silicon (Si) absorption coefficients, the optical path of the light inside the active layers of TF Si photovoltaic cells has to be increased to enhance the photogenerated current.[11] This can be achieved by introducing rough interfaces that induce a light trapping effect within the device. Another important parameter that qualifies an efficient TCO is a low resistivity, which has also been proven to be related to the size of the ZnO grains.[12] Therefore, the understanding and control of ZnO growth is of major interest to develop efficient layers to be used in photovoltaic cells.

The different phenomena that might govern polycrystalline growth of ZnO have already been investigated in ref 13, which is mainly based on results from sputtering experiments. However, little light has been shed up to now on the specific growing mechanisms of the LPCVD ZnO used in photovoltaic applications. In this letter, such a growth mechanism will be proposed on the basis of observations of ZnO growth of thin (40 nm) and thick (above 1.65 μm) layers at low (110 °C), intermediate (150 °C), and high (220 and 380 °C) growth temperatures (T_{growth}).

Experimental Details

ZnO films were deposited by LPCVD process on 4×4 cm^2 0.5 mm thick AF45 Schott glass substrates. Before deposition, the substrates were chemically cleaned with acid and base in ultrasonic baths. Diethylzinc (DEZ) and water (H_2O) vapors were used as precursors, and their flows were set to 16.2 and 32 sccm, respectively. Diborane (B_2H6) was used as doping gas, diluted at 1% in argon. The total pressure was kept at 0.5 mbar (~0.37 Torr) inside the reactor and the growth temperature was varied from 110 to 380 °C. The different samples were characterized with AFM and scanning electron microscopy to study the surface morphology, whereas XRD was used to determine the crystallographic orientations present at the different growth stages of the films.

Results and Discussion

It is well-known that several mechanisms, such as preferential nucleation and growth rate anisotropy of different crystal planes, can explain the apparition of texture in polycrystalline films. It has also been shown that the origin of textured surface is to be found either in the initial (nucleation) stage or in the growth stage.[13] In this work, the evolution of the crystallographic orientation with deposited thickness of films grown at 110 °C is first investigated. In Figure 1a, the $\log_{10}$ of the X-ray diffraction (XRD) intensity of LPCVD ZnO films with various thicknesses is plotted and each spectrum has been normalized to the maximum of the (0002) peak. Note that we have used the logarithm of the intensities in order to be able to identify even smaller features. It can be seen that for both thin and thick (1.7 and 3.5 μm) layers, the PO growth is along *c*-axis. In addition to the (0002) peak, several lower intensity features, such as $(10\bar{1}1)$ and $(10\bar{1}0)$, can also be observed in the thicker layer spectra. These peaks are ascribed to non *c*-axis oriented grains, which are

*Corresponding author. E-mail: sylvain.nicolay@epfl.ch. Phone: 0041 32 718 33 11.

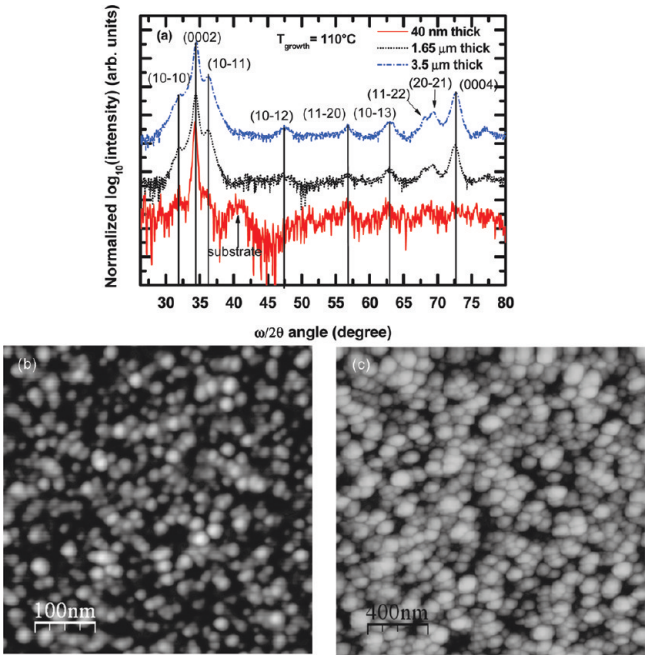

Figure 1. (a) XRD spectra of thin and thick films grown at 110 °C. (b) 0.5 × 0.5 μm^2 AFM picture on a 40 nm thick ZnO deposited at 110 °C. (c) 2 × 2 μm^2 AFM picture of a 1.65 μm thick ZnO deposited at 110 °C.

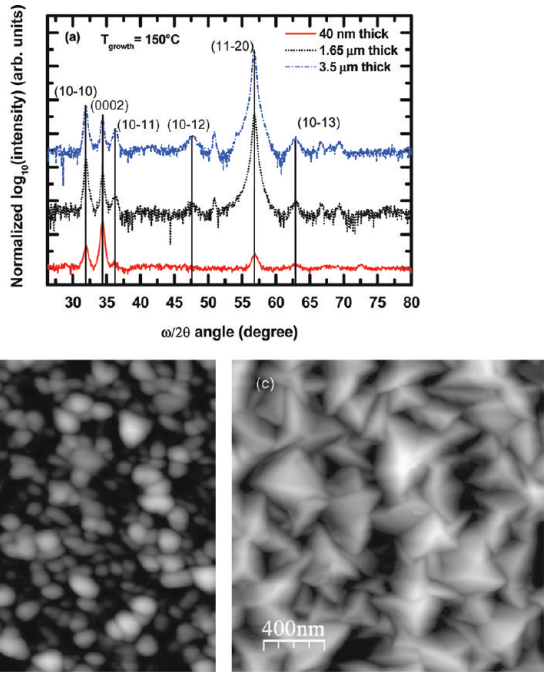

Figure 2. (a) XRD spectra of thin and thick films grown at 150 °C. (b) 0.5 × 0.5 μm^2 AFM picture on a 40 nm thick ZnO deposited at 150 °C. (c) 2 × 2 μm^2 AFM picture of a 1.65 μm thick ZnO deposited at 150 °C.

already present in the initial stage, although in small quantity as shown by the thin film XRD spectrum. The surface morphologies of the 110 °C grown films are shown in atomic force microscopy (AFM) pictures b and c in Figure 1 for 40 nm and 1.65 μm thick layers, respectively. Note that the surface morphology of the 3.5 μm thick layer is assumed to be similar to the one of the 1.65 μm thick film, but with larger grain size. Figure 1b is a 0.5 × 0.5 μm^2 scan with a rms value of 1.8 nm. It exhibits a surface made of small rounded grains. Figure 1c is a 2 × 2 μm^2 scan with a rms value of 10.2 nm, and it shows that the surface is constituted of larger grains but still with a rounded morphology. This rounded cap morphology observed for low T_{growth} (i.e., 110 °C), is typical of polycrystalline films deposited under condition of low adatom surface diffusion.[14]

XRD spectra of films with different thicknesses grown at 150 °C are shown in Figure 2a. As in the previous case, it can be seen that for the thin layer the PO is still along the *c*-axis and that other several weaker features are also present. Note that these smaller features are more marked than for the films deposited at 110 °C. However, when the film thickness is increased, the PO shifts from having (0002) planes parallel to the substrate, as it was the case at 110 °C, to (11$\bar{2}$0) planes being parallel to the surface as shown by the dominant intensity of the (11$\bar{2}$0) XRD peak for the 1.65 μm thick layer. When the thickness is further increased to 3.5 μm, the (11$\bar{2}$0) peak intensity becomes even more dominant, indicating that for thick layers grown at 150 °C the PO is well along *a*-axis and that it develops through the growth of the layer. AFM pictures taken on thin (40 nm) and thick (1.65 μm) layers are shown in images b and c in Figure 2, respectively. Figure 2b is a 0.5 × 0.5 μm^2 scan with a rms of 3.1 nm. It shows a surface made of more elongated and bigger grains than in the case of thin film deposited at low T_{growth} (Figure 1b). In Figure 2c, a 2 × 2 μm^2 scan characterized by a 52 nm rms shows a surface made of typical pyramids with stepped faces useful in TF photovoltaic solar cells for light scattering.[2]

Eventually, XRD spectra on thin and thick layers deposited at 220 °C are shown in Figure 3a. For the thin film, (10$\bar{1}$0) and (0002) are the dominant peaks, whereas (10$\bar{1}$1) and (11$\bar{2}$0) features appear with smaller intensities. When the thickness is increased at 1.65 μm, (11$\bar{2}$0) is the dominant XRD peak before (10$\bar{1}$0) and (10$\bar{1}$1), while the intensity of the (0002) peak becomes weaker. However, and contrary to the 150 °C case, when the thickness is increased to 4.3 μm, the highest peak becomes (10$\bar{1}$1). Although this is not evident on the plot of the logarithmic intensities, the inset of the figure presenting the linear intensity of the thickest layer, clearly shows that for the thicker film, the (10$\bar{1}$1) is indeed the PO. This indicates that, at 220 °C, a thicker film has to be deposited for the PO selection to occur. The surface morphologies of these layers can be seen in the AFM pictures presented in images b and c in Figure 3 for thin and thick layers, respectively. Figure 3b, a 0.5 × 0.5 μm^2 scan of the thin layer, shows that the surface is made of elongated grains with bigger size than in the 110 and 150 °C cases; its rms is 4 nm. Figure 3c is a 2 × 2 μm^2 scan of the 1.65 μm thick layer, and shows a shelf-structured surface with an rms of 54.4 nm.

Therefore, we have seen that in every case the PO in the initial layer is along the *c*-axis which is consistent with the lowest surface free energy of the (0002) plane in wurtzite ZnO.[15] Indeed, the classical theory of homogeneous nucleation shows that nuclei have to overcome an energy barrier, ΔG_c, in order to survive. This barrier is given for a spherical nucleus by $\Delta G_c = \frac{16\pi\gamma^3}{3(\Delta G_v)^2}$ where ΔG_v is the difference between the chemical potential of the vapor and crystalline phase per unit volume and γ is the surface free energy of the film. In the case of heterogeneous nucleation, as we are dealing with in this work, the energy barrier becomes $\Delta G_c^* = \frac{1}{4}(2+\cos\theta)(1-\cos\theta)^2 \frac{16\pi\gamma_{fv}^3}{3(\Delta G_v)^2}$ with $\cos\theta = \frac{\gamma_{sv}-\gamma_{sf}}{\gamma_{fv}}$ where γ_{sv}

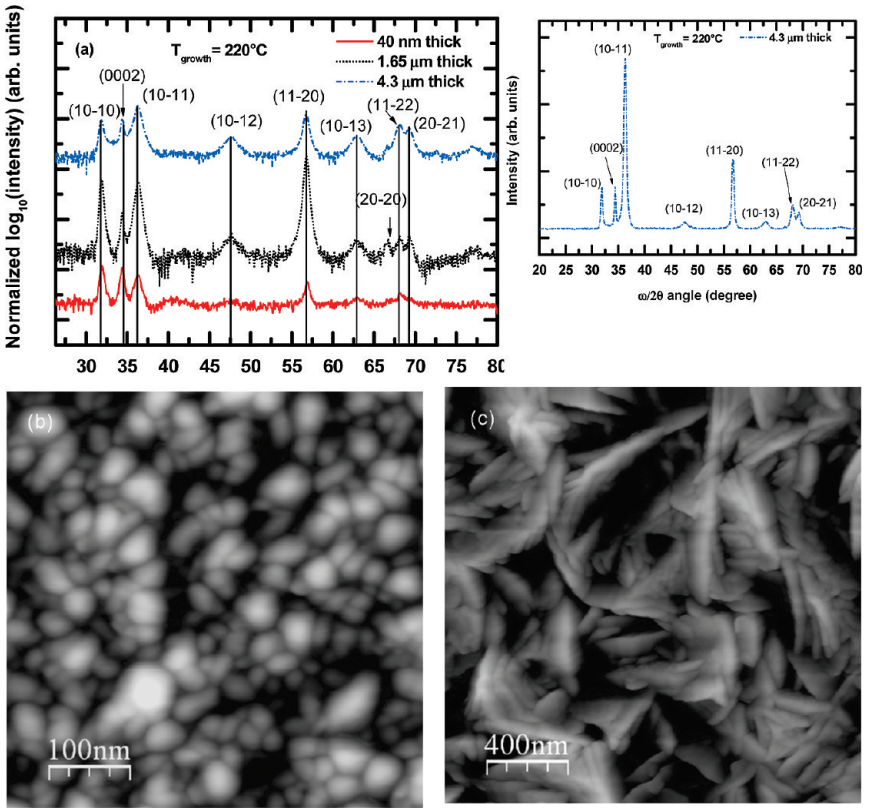

Figure 3. (a) XRD spectra of thin and thick films grown at 220 °C. Inset: linear intensity of the XRD on the thickest layer. (b) $0.5 \times 0.5\ \mu m^2$ AFM picture on a 40 nm thick ZnO deposited at 220 °C. (c) $2 \times 2\ \mu m^2$ AFM picture of a 1.65 μm thick ZnO deposited at 220 °C.

is the surface energy of the substrate, γ_{sf} is the interfacial energy between the substrate and the film, and γ_{fv} is the surface energy of the nucleus. From these equations, it is seen that $\cos\theta = 1$ gives the lowest nucleation barrier.[16] As a consequence, grains with the lowest surface free energy, γ_{fv}, should be favored in the nucleation process. However, our growth conditions are far from thermodynamic equilibrium, notably for the low T_{growth} values, which leads to the apparition of nonminimum surface free energy (NMSE) grain in the initial layer as seen in the various XRD spectra of thin and thick films.

Furthermore, the apparition of different POs at 150 and 220 °C when the film thickness is increased also points toward nonthermodynamically driven growth and rather indicates the predominance of kinetic growth phenomena. Indeed, the fact that a certain growth orientation emerges from the initial layer, in which it is not the dominant one, is typical of the evolutionary selection theory based on kinetic growth aspects.[17,18] Evolutionary selection relies on the growth rate anisotropy of the different crystallographic planes of a material. It states that the grains having the fastest growing direction perpendicular to the surface will survive through the growth and becomes PO, e.g., in our case, this would correspond to the $(11\bar{2}0)$ planes at 150 °C or the $(10\bar{1}1)$ planes at 220 °C. On the basis of this theory, it is proposed that the PO and morphology evolutions with the thickness observed on films grown at different T_{growth} values are attributed to temperature-activated growth rate anisotropy of the different ZnO crystallographic plane orientations. As a consequence and depending on T_{growth}, some initial clusters with given planes parallel to the substrate surface would grow faster and at the expense of other grains characterized by a slower vertical growth rate at this temperature. In fact, such a variation in the PO at different temperatures has already been reported in the literature for MOCVD and sputtered grown ZnO.[19−21]

To have a better understanding of the different phenomena that could lead to such growth rate anisotropy in our case, we present a schematic drawing of the situation for different T_{growth} values in Figure 4. In this figure, two initial clusters are considered with different crystallographic orientations parallel to the substrate surface, nonminimum surface free energy (NMSE) and minimum surface free energy (MSE) planes. For the sake of simplicity, we consider the case of rectangular-shaped clusters in which the NMSE and MSE orientations are orthogonal, as is the case in wurtzite ZnO for the [0002] and $[11\bar{2}0]$ directions.

At low T_{growth} (110 °C), the adatoms surface mobility is low. As a consequence, adatoms arriving on the substrate surface are characterized by a low diffusion length and they have the tendency to create new clusters with the PO (0002) because of surface free energy minimization, as indicated by the XRD spectra of thin layers where the (0002) peak is dominant. Regarding adatoms arriving on the grain with NMSE planes parallel to the substrate, they will also have the tendency to stick at their arrival place because of their low mobility and the higher dangling bond (DB) density associated with NMSE planes.[22,23] Indeed, the surface free energy can be seen as the excess energy of surface atoms due to the presence of broken bonds at this surface. Therefore, it is intuitive that facets with higher surface free energy have a higher DB density.[24] This phenomenon contributes to the vertical growth of the grains with NMSE planes parallel to the substrate. On the contrary, adatoms arriving on MSE facets have a higher surface diffusivity due to the lowest DB density of the arrival planes. Therefore, some of these adatoms have the possibility to move to the edge of the clusters where the DB

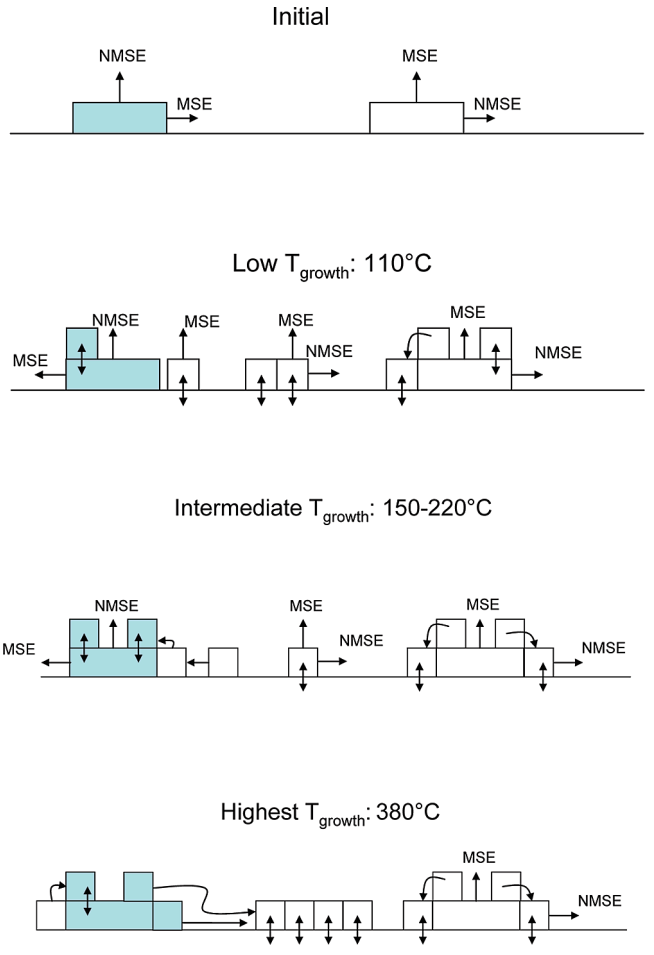

Figure 4. Schematic drawing of PO selection mechanisms at different T_{growth} values.

density is higher (as the lateral face is a NMSE plane), which contributes to their lateral expansion. However, this lateral expansion should be limited because of the low T_{growth}. In addition, as it has been observed that at T_{growth} = 110 °C the PO is (0002) for thin and thick layers, it is proposed that the larger amount of clusters forming with the MSE, (0002), planes and their higher lateral growth rate dominates the few clusters with NMSE planes parallel to the substrate, which grow vertically at an insufficient rate to shadow the growth of the MSE clusters. In fact, it is supposed that the vertical growth rate of both MSE and NMSE clusters are similar at low T_{growth}.

At intermediate T_{growth} (150−220 °C), the adatoms have a higher surface mobility due to the higher temperature. Hence, instead of creating new MSE clusters, adatoms arriving close to the edge of the NMSE grains have the possibility to diffuse from their lateral MSE facets, characterized by a low DB density, and to jump on the NMSE planes of these grains where the DB density is higher. As a consequence of this interfacet diffusion, the NMSE clusters have a higher adatom concentration on their NMSE facets, resulting in a higher vertical growth rate compared to the low T_{growth} case but also compared to their own lateral growth rate.[22,23] It is also interesting to note that by piling up atoms vertically, the exposed surface of NMSE planes is not increased while the size of their lateral MSE facets is increased, which also contributes to a minimization of the grain surface free energy.[25] Regarding initial cluster with MSE planes parallel to the substrate, the higher adatom surface diffusivity due to both the higher T_{growth} and to the lower DB density of these planes, leads to a decreased adatom density on their horizontal surfaces, which decreases their vertical growth rate. In this case, the increased vertical growth rate of the NMSE clusters dominates the vertical and lateral expansion of the grains with MSE planes parallel to the substrate. Therefore, as predicted by the evolutionary selection, clusters that have the NMSE planes parallel to the substrate in the initial stage will survive through the growth. This explains why the $(11\bar{2}0)$ peak of the XRD spectrum of the films grown at 150 °C (the peak that corresponds to NMSE planes parallel to the surface) has first a smaller intensity relatively to the other peaks of the thin layer, and then becomes the dominant crystallographic orientation in the thick layers. Such a grain growth competition also leads to the peculiar TEM structures observed in ref 10, where some grains emerge at the surface while being enclosed by others.[26] The predominance of NMSE clusters that have a higher vertical growth rate than their own lateral growth rate also explains the stepped pyramidal shape of the surface features characteristic of the thick layers grown in this temperature range. Regarding the layers deposited at 220 °C, the emergence of the $(10\bar{1}1)$ peak in the XRD spectrum of a thick layer is ascribed to the increase in the adatom surface mobility because of the higher T_{growth}, leading to the selection of NMSE with another PO as the thickness is increased. It also seems that the growth competition between differently oriented NMSE clusters leads to the fact that one needs to deposit a thicker layer to see a definitive PO emerging at this temperature. The increased adatom mobility can also explain why in thin layer deposited at 150 and 220 °C, XRD spectra show several peaks with intensities comparable to the one of the (0002) feature. Indeed, as explained before, because of their higher diffusive ability, adatoms can jump on the surface of NMSE clusters instead of forming new grains directly on the substrate with (0002) planes parallel to the surface; this in turn reduces the relative intensity of the *c*-axis peak and increases the one of the NMSE clusters.

To summarize, it is proposed that depending on the surface mobility of the arriving adatoms (which is increased as the growth temperature is increased), interfacets diffusion can occur, which leads to the fact that grains with NMSE planes parallel to the surface have a dominant vertical growth rate allowing them to emerge through the growth. To further test this hypothesis, we have deposited thin (50 nm) and thick layers (1.7 and 3 μm) at 220 °C with reduced flows of DEZ and H_2O, which were respectively set to 10 and 20 sccm in order to keep a H_2O/DEZ ratio similar to the one used for the deposition of the previous films. By decreasing the reactant flows, it is assumed that the adatom mobility is increased as the surface atoms have more possibility to move before being frozen by new incoming atoms. In accordance with an adatom mobility-driven PO selection process, the increased adatom surface mobility led to the apparition of a new NMSE PO, $(11\bar{2}2)$, in the deposited film, as shown in the XRD spectra of Figure 5.

Again, in this figure it can be seen that several orientations are dominant in the initial stage, whereas the $(11\bar{2}2)$ orientation becomes PO only as the thickness is increased. In addition, the apparition of this new PO by simply changing the flow rates also discards the possibility that we are dealing with a chemically driven PO growth in which ionic radicals that would be present at different T_{growth} in the vapor phase would inhibit certain growth directions, as was proposed in ref 27.

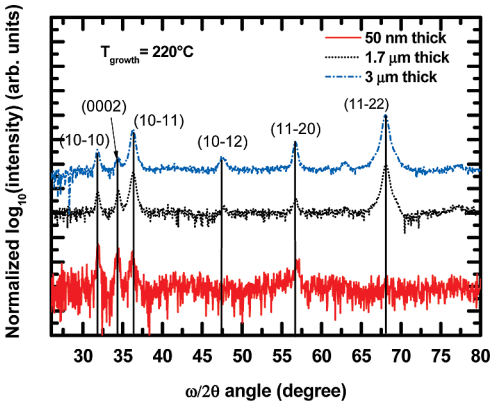

Figure 5. XRD spectra of thin and thick films grown at 220 °C with lower precursor gas flows.

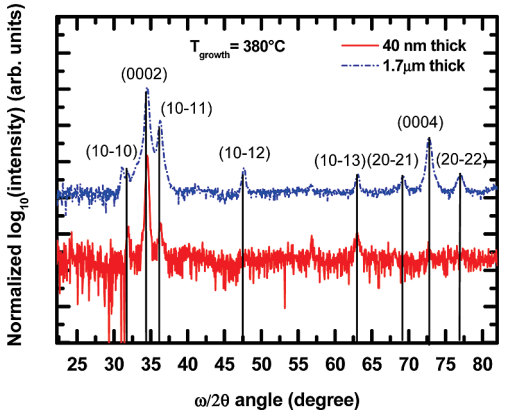

Figure 6. XRD spectra of thin and thick films grown at 380 °C.

Note that it is assumed that as the deposition is carried out at low pressure, variations in gas flows do not influence the vapor phase reactions. Eventually, it is predicted that if the adatom surface mobility is further increased, the PO should go back to having the MSE planes parallel to the substrate.[22,25] Indeed, as schematized in the last drawing of Figure 4, if the substrate temperature is increased to the point where the adatoms have sufficient mobility to overcome the high DB density of the horizontal face of the NMSE clusters, they will have a tendency to diffuse to the edge of MSE grains (intergrain diffusion), where they could attach in order to decrease the surface free energy of the whole system. In this case, the intergrain diffusion becomes dominant compared to the intragrain (or interfacet) diffusion present at lower T_{growth}. As a consequence, the adatom concentration on the surface of NMSE clusters will decrease, leading to a lower vertical growth rate, thus the *c*-axis orientation of enlarged MSE grains should become again the PO of the film. This is experimentally confirmed, as shown in Figure 6, which exhibits the XRD spectra of thin (40 nm) and thick (1.7 μm) layers grown at 380 °C.

As expected, the (0002) orientation is again the PO in both thin and thick layers. This indicates well that the *c*-axis oriented grains are dominant from the nucleation stage and throughout the growth. Eventually it has to be pointed out that by further increasing the adatom diffusivity, e.g by decreasing the precursor flows at high T_{growth}, the only orientation present in the film through the entire growth should be (0002) as Ostwald ripening in the nucleation stage should remove every NMSE clusters from the growth. To conclude this discussion, it is important to remind that similar PO selections based on interfacet and intergrain diffusion, depending on the adatom mobility at different growth temperatures, have been reported in refs 21 and 28 for sputtered ZnO and GaN, respectively.

Conclusions

In conclusion, the orientation and surface morphology evolution of LPCVD grown ZnO layers have been studied on thin and thick films grown at different temperatures. It is shown that the films PO evolves from *c*-axis to *a*-axis as the growth temperature is increased from 110 to 220 °C and then goes back to *c*-axis at 380 °C.From these observations, a mechanism explaining the growth of LPCVD polycrystalline ZnO thin film is proposed. This mechanism is based on the temperature dependent selection of different PO present in the initial layer. This selection occurs through evolutionary selection of certain grains, which can have increased vertical growth rate depending on their surface adatom mobility. This work can help us understand the variety of results presented up to now in the literature and help explain the different orientations observed in ZnO growth. In addition, the understanding of polycrystalline LPCVD ZnO growth is a first step toward the possibility to improve these layers for photovoltaic applications.

Acknowledgment. The authors acknowledge financial support from the Swiss Federal Office for Energy (OFEN) and Dr. Neels from CSEM in Neuchâtel for XRD spectra.

References

(1) Bagnall, D. M.; Chen, Y. F.; Zhu, Z.; Yao, T.; Koyama, S.; Shen, M. Y.; Goto, T. *Appl. Phys. Lett.* **1997**, *70*, 2230.
(2) Fay, S.; Feitknecht, L.; Schluchter, R.; Kroll, U.; Vallat-Sauvain, E.; Shah, A. *Sol. Energy Mater. Sol. Cells* **2006**, *90*, 2960.
(3) Saitoh, H.; Satoh, M.; Tanaka, N.; Ueda, Y.; Ohshio, S. *Jpn. J. Appl. Phys.* **1999**, *38*, 6873.
(4) Kluth, O.; Schope, G.; Hupkes, J.; Agashe, C.; Muller, J.; Rech, B. *Thin Solid Films* **2003**, *442*, 80.
(5) Chen, Y.; Ko, H.-J.; Hong, S.-K.; Segawa, Y.; Yao, T. *Appl. Phys. Lett.* **2002**, *80*, 1358.
(6) Ohyama, M.; Kozuka, H.; Yoko, T. *J. Am. Ceram. Soc.* **1998**, *81*, 1622.
(7) Meier, J.; Spitznagel, J.; Kroll, U.; Bucher, C.; Fay, S.; Moriarty, T.; Shah, A. *Thin Solid Films* **2004**, *451*, 518.
(8) Buehlmann, P.; Bailat, J.; Dominé, D.; Billet, A.; Meillaud, F.; Feltrin, A.; Ballif, C. *Appl. Phys. Lett.* **2007**, *91*, 143505.
(9) Dominé, D.; Buehlmann, P.; Bailat, J.; Billet, A.; Feltrin, A.; Ballif, C. *Rapid Res. Lett.* **2008**, *2*, 163.
(10) Fay, S.; Steinhauser, J.; Oliveira, N.; Vallat-Sauvain, E.; Ballif, C. *Thin Solid Films* **2007**, *515*, 8558.
(11) Meier, J.; Kroll, U.; Dubail, S.; Golay, S.; Fay, S.; Dubail, J.; Shah, A. *Proceedings of the 28th IEEE Photovoltaic Specialists Conference*; IEEE: Piscataway, NJ, 2000; p 746
(12) Steinhauser, J.; Fay, S.; Oliveira, N.; Vallat-Sauvain, E.; Ballif, C. *Appl. Phys. Lett.* **2007**, *90*, 142107.
(13) Kajikawa, Y. *J. Cryst. Growth* **2006**, *289*, 387.
(14) Thornton, J. A. *Annu. Rev. Mater. Sci.* **1977**, *7*, 239.
(15) Fujimura, N.; Nishihara, T.; Goto, S.; Xu, J.; lto, T. *J. Cryst. Growth* **1993**, *130*, 269.
(16) Fujihara, S.; Sasaki, C.; kimura, T. *Appl. Surf. Sci.* **2001**, *180*, 341.
(17) Van Der Drift, A. *Phillips Res. Rep.* **1967**, *22*, 267.
(18) Kajikawa, Y.; Noda, S.; Komiyama, H. *Mater. Sci. Eng., B* **2004**, *111*, 156.
(19) Fay, S.; Kroll, U.; Bucher, C.; Vallat-Sauvain, E.; Shah, A. *Sol. Energy Mater. Sol. Cells* **2005**, *86*, 385.
(20) Chen, X. L.; Geng, X. H.; Xue, J. M.; Zhang, D. K.; Hou, G. F.; Zhao, Y. *J. Cryst. Growth* **2006**, *296*, 43.

(21) Singh, S.; Ganguli, T.; Kumar, R.; Srinivasa, R. S.; Major, S. S. *Thin Solid Films* **2008**, *517*, 661.
(22) Huang, H.; Gilmer, G. H.; de la Rubia, T. D. *J. Appl. Phys.* **1998**, *84*, 3636.
(23) Wang, Z.; Li, Y.; Adams, J. B. *Surf. Sci.* **2005**, *450*, 51.
(24) Zhang, S. B.; Wei, S.-H. *Phys. Rev. Lett.* **2004**, *92*, 086102.
(25) Kajikawa, Y.; Noda, S.; Komiyama, H. *J. Vac. Sci. Technol. A* **2003**, *21*, 1943.
(26) Kajikawa, Y. *Mater. Chem. Phys.* **2008**, *112*, 311.
(27) Pung, S. Y.; Choy, K. L.; Hou, X.; Shan, C. *Nanotechnology* **2008**, *19*, 435609.
(28) Yadav, B. S.; Major, S. S.; Srinivasa, R. S. *J. Appl. Phys.* **2007**, *102*, 073516.